Lung Cancer 129 (2019) 80–84

Contents lists available at ScienceDirect

Lung Cancer

journal homepage: www.elsevier.com/locate/lungcan

# Imaging characteristics of BRAF-mutant non-small cell lung cancer by functional class

Dexter P. Mendoza[a,1], Ibiayi Dagogo-Jack[b,1], Tianqi Chen[c], Atul Padole[a], Jo-Anne O. Shepard[a], Alice T. Shaw[b], Subba Rao Digumarthy[a,*]

[a] Department of Radiology, Massachusetts General Hospital, United States
[b] Massachusetts General Hospital Cancer Center and Department of Medicine, Massachusetts General Hospital, United States
[c] Department of Biostatistics and Computational Biology, Dana-Farber Cancer Institute, Harvard Medical School, United States

ARTICLE INFO

*Keywords:*
Lung cancer
BRAF mutation
Radiology
Imaging
Metastasis

ABSTRACT

*Objectives:* Mutations in the BRAF gene have emerged as a validated molecular target in the treatment of non-small cell lung cancer (NSCLC). These mutations can be classified into three functional classes based on their mechanisms of oncogenesis. The relationship between these functional classes and their imaging features has not been systematically investigated. The goal of this work is to determine if imaging features of the primary tumor and the pattern of metastasis correlate with the functional class of BRAF mutation.

*Methods:* We reviewed pre-treatment computed tomography (CT) images of patients with BRAF-mutated NSCLC with known functional class. We assessed and recorded the features of the primary tumor and the patterns of lymphadenopathy and distant metastasis. Wilcoxon rank-sum test and Kruskal-Wallis test were performed to compare continuous characteristics, and Fisher's exact test was used to compare categorical features between groups.

*Results and Conclusions:* 105 patients with BRAF-mutant NSCLC had pre-treatment imaging available for review (n = 43 class I, n = 40 class II, and n = 22 class III). Approximately half of the primary tumors were considered masses (n = 54/105, 51%) and most were solid (n = 81/105, 77%). There were no statistically significant differences in imaging features of the primary tumor among the three functional classes. Intrathoracic metastases occurred more frequently in class I tumors compared to tumors with class II and III mutations (p = 0.03). The odds of class I mutation were higher among tumors involving the pleural space (OR: 4.39, 95% CI: 1.11–17.4) and lower among tumors disseminating to the abdomen (OR: 0.25, 95% CI: 0.07-0.92). Our findings suggest that class I (V600) mutated NSCLC may be more likely to have intrathoracic metastases, while classes II and III (non-V600) mutated NSCLC may be more likely to have intra-abdominal metastases at the time of presentation.

## 1. Introduction

*BRAF* mutations are a promising target in lung cancer [1]. In non-small cell lung cancer (NSCLC), nearly half of *BRAF* mutations lead to a substitution of valine for glutamic acid at codon 600 (V600E) [1,2].Based on the prevalence of this substitution, *BRAF* mutations were historically classified as either V600-mutant or non-V600 mutant. Emerging data demonstrating a link between specific *BRAF* variants and degree of RAF kinase activation has allowed for further stratification of *BRAF* mutations into three functional classes [3,4]. Class I consists of V600 mutations that enable RAS-independent, monomeric signaling. In contrast, classes II and III both signal as dimers and are distinguished by RAS dependence and RAF kinase activity. Specifically, class II *BRAF* mutants result in high kinase activity and RAS-independent signaling whereas RAS-dependent class III mutants are characterized by impaired RAF kinase activity [3,5].

We recently demonstrated that the clinical outcome of patients with metastatic NSCLC is impacted by *BRAF* functional class [6]. Here, we build upon this initial observation by systematically analyzing the imaging features of *BRAF*-mutant NSCLC to explore whether mutation class correlates with features of the primary lung tumor or distribution of metastases sites.

* Corresponding author at: Department of Radiology, Massachusetts General Hospital, 55 Fruit Street, Founders 202, Boston, MA, 02114, United States.
*E-mail address:* sdigumarthy@mgh.harvard.edu (S.R. Digumarthy).
[1] These authors contributed equally to this manuscript.

https://doi.org/10.1016/j.lungcan.2019.01.007
Received 2 December 2018; Received in revised form 12 January 2019; Accepted 16 January 2019

## 2. Methods

### 2.1. Study population

Patients (n = 105) with BRAF-mutant NSCLC were identified from NSCLCs that underwent molecular analysis at Massachusetts General Hospital from 2005 -2017. *BRAF* mutations were identified using SNaPshot as previously described [7]. The current version of SNaPshot utilizes next-generation sequencing to interrogate exons 11 and 15 of *BRAF*, whereas versions launched prior to 2014 relied on multiplex polymerase chain reaction technology. We organized *BRAF* mutations into three functional classes (n = 43 class I, n = 40 class II, and n = 22 class III) based on the published preclinical studies that validated kinase activity of distinct mutations [3,4]. Only patients with available pretreatment scans were included. This study was approved by the Massachusetts General Hospital Institutional Review Board.

### 2.2. Imaging protocol

As our institution is a tertiary referral center, thirty-four (32.3%) patients had pretreatment imaging performed at an outside facility. For these patients, baseline imaging was obtained with a variety of multidetector-row CT scanners from different vendors. Examinations performed at our institution were acquired helically with automatic exposure control and tube potential of 100 −120 kV. At a minimum, images consisted of standard soft tissue kernel reconstructions with slice thickness of 1–3 mm for the chest and up to 5 mm for the abdomen and pelvis with sagittal and coronal reformatted images. Eighty-four (80%) studies were performed with intravenous contrast. When available, brain MRI, head CT, and FDG-PET images were reviewed for the presence of intracranial metastases and occult metastases. Pretreatment brain imaging was available in 88 (83.8%) patients, and FDG-PET imaging was available in and FDG-PET were available in 92 (87.6%) patients.

### 2.3. Image review and analysis

Images were reviewed on our institutional PACS (AGFA Impax 6, Mortsel, Belgium) by both a fellowship-trained, board-certified thoracic radiologist (SRD) and a thoracic imaging fellow (DM). Radiologists were blinded to *BRAF* class at the time of imaging review. Images were reviewed concurrently, and assessments were derived through consensus. The review included assessment of the primary tumor [size, location within the lobe (inner, middle, or outer third), density (solid, mixed, ground-glass), cavitation, air bronchograms, and calcifications], evaluation for presence of lymphangitic carcinomatosis (i.e., thickening and nodularity of the septal interstitium extending beyond the primary tumor and involving greater than half a lobe), and location of metastatic lymph nodes. Lymph nodes were considered malignant if greater than 1 cm in the short axis or associated with increased FDG uptake. The presence of metastasis in the lungs, pleura, liver, adrenal glands, other viscera and soft tissues, bones, and brain was also documented for each patient. Imaging findings were correlated with surgical pathology when available to verify nodal and distant metastases.

### 2.4. Statistical analysis

The Wilcoxon rank-sum test and Kruskal-Wallis test were performed to compare continuous characteristics between groups. Fisher's exact test was used to compare categorical features between groups. All tests were two-sided and p-value was considered significant if less than 0.05. A multivariable logistic regression model was built with V600 as outcome. The criterion for choosing candidate predictors was based on univariate analysis p-value < 0.20.

## 3. Results

### 3.1. Patient characteristics

We reviewed baseline imaging studies from 105 patients with *BRAF*-mutant NSCLC. Over one-half of the patients had stage IV adenocarcinoma. There was no significant difference between the three classes with respect to age, sex, ethnicity, histology, or stage at diagnosis. However, as previously observed, there was a difference in smoking status between V600-mutated versus non-V600-mutated patients [6]. Clinicopathologic characteristics and class comparisons are summarized in Supplement 1.

### 3.2. Imaging characteristics of BRAF-mutant NSCLC

#### 3.2.1. Primary tumor

Approximately one-half of the *BRAF*-mutant tumors were categorized as masses (i.e. greater than 3 cm in greatest axial dimension; n = 54/105, 51%). Eighty-one (77%) of the tumors were solid. Air bronchograms, cavitation, and calcification were rare with incidences of 5%, 2%, and 2%, respectively. Twenty-five (24%) patients had multifocal lung tumors at baseline. Lymphangitic carcinomatosis was observed in eight (8%) cases. When the classes were compared, differences in imaging features of the primary tumor did not reach statistical significance (Table 1).

#### 3.2.2. Lymphadenopathy and metastatic patterns

Fifty-three (50.4%) patients had nodal disease at diagnosis, including 28 (26.7%) patients with enlarged or hypermetabolic N3 nodes. The pattern of lymphadenopathy was consistent across the three functional classes. Notably, intrathoracic metastases (lung and pleural lesions) occurred more frequently in class I tumors compared to tumors with class II and III mutations (44% vs 28% vs 14%, p value = 0.03; Fig. 1). The distribution of nodal and extrathoracic metastases is detailed in Table 1.

In a multivariable logistic regression model that accounted for smoking status, N3 nodal status, tumor calcification, lung metastases, pleural involvement, and intra-abdominal metastasis, pleural and intra-abdominal metastasis were significant predictors of *BRAF* mutation class. When tumors with class II and III mutations were pooled and the analysis was adjusted for the other covariates, the odds of class I mutation among tumors involving the pleural space, were more than four-fold higher than those not involving the pleural space (OR: 4.39, 95% CI: 1.11–17.4), and 75% lower among tumors disseminating to the abdomen compared to those not disseminating to the abdomen (OR: 0.25, 95% CI: 0.07-0.92) (Supplement 2). The receiver operating characteristic (ROC) curve for the multivariable logistical regression model is shown in Supplement 3 A. For comparison, an ROC curve taking into account only clinical characteristics is shown in Supplement 3B.

## 4. Discussion

Elucidation of the distinct mechanisms of oncogenesis of different BRAF mutations has improved understanding of the heterogeneity within the non-V600 subset. Class II BRAF mutations result in high kinase activity and RAS-independent signaling and include mutations in the K601, L597 V/Q/R, G469 V/S/R/E/A, and G464 V codons. On the other hand, class III mutations are RAS–dependent and have impaired RAF kinase activity and include mutations in the G596R, D594Y/N/G/E, N581Y/S/I, G466 V/L/E/A, and D287Y codons [3,5]. A recent retrospective analysis of over 200 patients with BRAF-mutant NSCLC suggested that the biological differences between functional classes may translate into differences in clinical outcomes and survival among patients with metastatic NSCLC [6]. Considering the above, we conducted this imaging-based study to evaluate for a link between

**Table 1**
Imaging features of BRAF-mutated tumors and comparison among classes.

| | | Mutation class | | | P-value | |
|---|---|---|---|---|---|---|
| | All (N = 105) | Class I (N = 43) | Class II (N = 40) | Class III (N = 22) | Class I vs. II vs. III | V600 vs. Non-V600 |
| **Median (range)** | | | | | | |
| **Tumor size, mm** | | | | | | |
| Maximum dimension | 32 (7-130) | 25 (9-130) | 38 (10-110) | 22 (7-69) | ***0.01*** | 0.35 |
| **N (%)** | | | | | | |
| **Tumor size (maximum)** | | | | | | |
| 0-3 cm | 51 (49%) | 24 (56%) | 14 (35%) | 13 (59%) | 0.23 | 0.37 |
| 3-5 cm | 29 (28%) | 9 (21%) | 14 (35%) | 6 (27%) | | |
| > 5 cm | 25 (24%) | 10 (23%) | 12 (30%) | 3 (14%) | | |
| **Location** | | | | | | |
| Multifocal | 25 (24%) | 11 (26%) | 8 (20%) | 6 (27%) | 0.76 | 0.82 |
| Non multifocal | 80 (76%) | 32 (74%) | 32 (80%) | 16 (73%) | | |
| **Zone** | | | | | | |
| Inner | 57 (54%) | 24 (56%) | 24 (60%) | 9 (41%) | 0.11 | 0.53 |
| Middle | 20 (19%) | 6 (14%) | 5 (12%) | 9 (41%) | | |
| Outer | 28 (27%) | 13 (30%) | 11 (28%) | 4 (18%) | | |
| **Density** | | | | | | |
| GG | 13 (12%) | 4 (9%) | 4 (10%) | 5 (23%) | 0.40 | 0.45 |
| Mixed | 11 (10%) | 3 (7%) | 5 (12%) | 3 (14%) | | |
| Solid | 81 (77%) | 36 (84%) | 31 (78%) | 14 (64%) | | |
| **Air bronchogram or cavitation** | | | | | | |
| No | 98 (93%) | 39 (91%) | 37 (92%) | 22 (100%) | 0.52 | 0.44 |
| Yes | 7 (7%) | 4 (9%) | 3 (8%) | 0 (0%) | | |
| **Tumor Calcification** | | | | | | |
| No | 103 (98%) | 41 (95%) | 40 (100%) | 22 (100%) | 0.51 | 0.17 |
| Yes | 2 (2%) | 2 (5%) | 0 (0%) | 0 (0%) | | |
| **Lymphangitic carcinomatosis** | | | | | | |
| No | 97 (92%) | 39 (91%) | 37 (92%) | 21 (95%) | 0.90 | 0.71 |
| Yes | 8 (8%) | 4 (9%) | 3 (8%) | 1 (5%) | | |
| **N1** | | | | | | |
| No | 52 (50%) | 24 (56%) | 16 (40%) | 12 (55%) | 0.30 | 0.32 |
| Yes | 53 (50%) | 19 (44%) | 24 (60%) | 10 (45%) | | |
| **N2** | | | | | | |
| No | 59 (56%) | 22 (51%) | 21 (52%) | 16 (73%) | 0.23 | 0.43 |
| Yes | 46 (44%) | 21 (49%) | 19 (48%) | 6 (27%) | | |
| **N3** | | | | | | |
| No | 74 (70%) | 27 (63%) | 28 (70%) | 19 (86%) | 0.14 | 0.19 |
| Yes | 31 (30%) | 16 (37%) | 12 (30%) | 3 (14%) | | |
| **Intrathoracic Metastasis** | | | | | | |
| No | 72 (69%) | 24 (56%) | 29 (72%) | 19 (86%) | ***0.04*** | ***0.03*** |
| Yes | 33 (31%) | 19 (44%) | 11 (28%) | 3 (14%) | | |
| **Lung Metastasis** | | | | | | |
| No | 80 (76%) | 29 (67%) | 31 (78%) | 20 (91%) | 0.11 | 0.10 |
| Yes | 25 (24%) | 14 (33%) | 9 (22%) | 2 (9%) | | |
| **Pleural Metastasis** | | | | | | |
| No | 91 (87%) | 34 (79%) | 36 (90%) | 21 (95%) | 0.16 | 0.08 |
| Yes | 14 (13%) | 9 (21%) | 4 (10%) | 1 (5%) | | |
| **Extrathoracic Metastasis** | | | | | | |
| No | 73 (70%) | 31 (72%) | 26 (65%) | 16 (73%) | 0.76 | 0.67 |
| Yes | 32 (30%) | 12 (28%) | 14 (35%) | 6 (27%) | | |
| **Intra-abdominal metastasis** | | | | | | |
| No | 85 (81%) | 38 (88%) | 28 (70%) | 19 (86%) | 0.10 | 0.13 |
| Yes | 20 (19%) | 5 (12%) | 12 (30%) | 3 (14%) | | |
| **Bone Metastases** | | | | | | |
| No | 91 (87%) | 38 (88%) | 34 (85%) | 19 (86%) | 0.93 | 0.78 |
| Yes | 14 (13%) | 5 (12%) | 6 (15%) | 3 (14%) | | |
| **Brain Metastasis** | | | | | | |
| No | 99 (94%) | 39 (91%) | 40 (100%) | 20 (91%) | 0.11 | 0.22 |
| Yes | 6 (6%) | 4 (9%) | 0 (0%) | 2 (9%) | | |

aggressive imaging features—such as large tumor size and specific metastatic site tropisms— and the class of *BRAF* mutation. Our findings suggest that lung tumors with class I *BRAF* mutations are more likely to involve the pleural space and less likely to present with intra-abdominal metastases.

In the present study, we did not identify differences in imaging features of the primary tumor across *BRAF* functional classes. Our findings are consistent with a smaller study by Halpenny et al, which similarly failed to detect differences in the imaging features of primary lung tumors bearing non-V600-mutant and V600-mutant *BRAF* mutations [8]. Beyond investigating this question in a larger group of patients, our study adds to the previous analysis by separating the non-V600 group into biologically-relevant functional classes. In both our study and the earlier study by Halpenny, *BRAF*-mutant NSCLCs largely presented as solid masses or nodules. Interestingly, this finding contrasts with *EGFR*-mutant NSCLC, which is associated with increased prevalence of ground-glass components [9].

We observed notable differences in the metastatic patterns of specific functional classes. As metastasis is the primary determinant of mortality from NSCLC, this finding may have larger prognostic

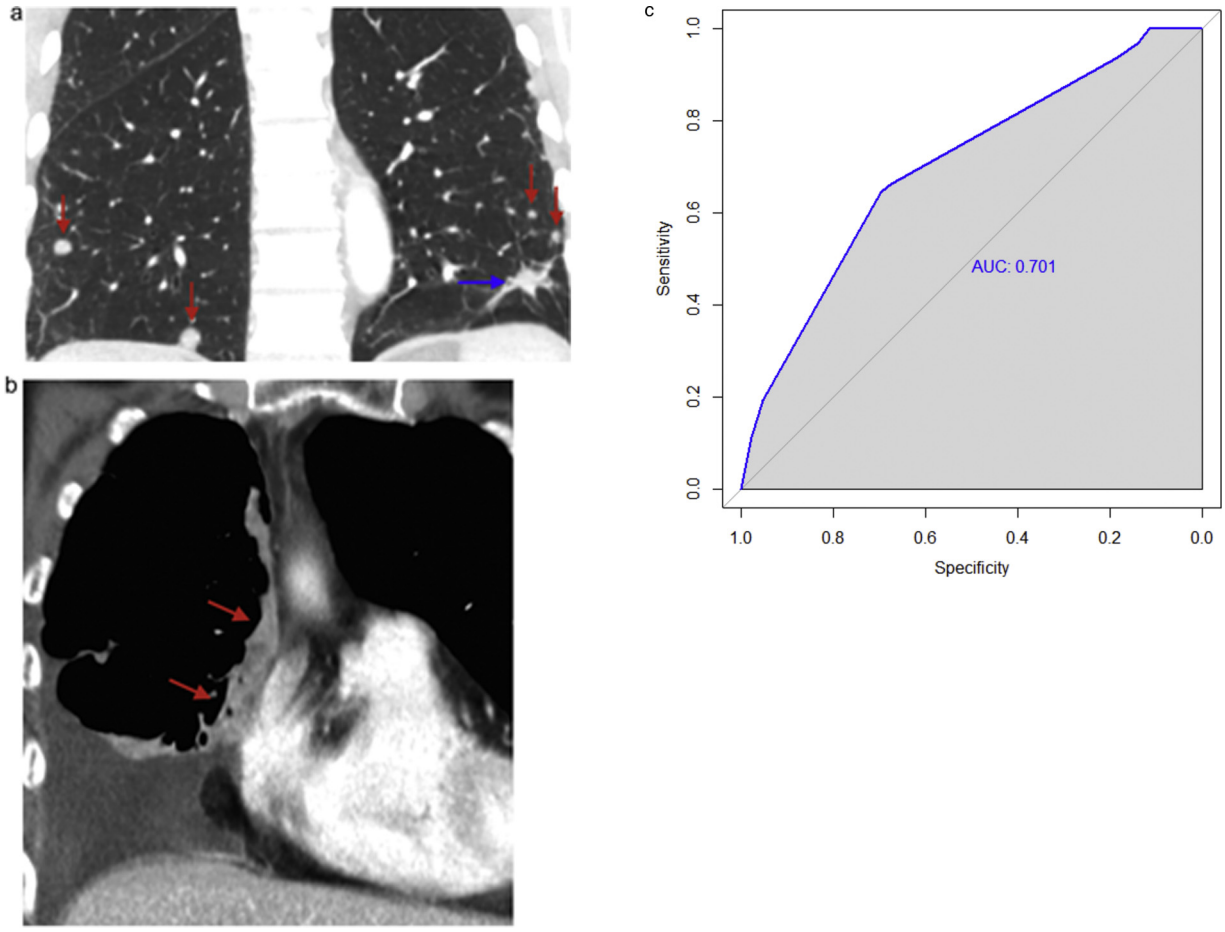


**Fig. 1.** Intrathoracic metastases in V600 mutant NSCLC. (A) Coronal CT of a patient with V600-mutant NSCLC demonstrates spiculated nodule in the left lower lobe (blue arrow) with bilateral lung metastases (red arrows). (B) Coronal CT image of a different patient with V600-mutant NSCLC demonstrates pleural metastasis (red arrows) and associated malignant pleural effusion. The primary lesion is not shown. (For interpretation of the references to colour in this figure legend, the reader is referred to the web version of this article).

implications than comparison of characteristics of the initiating tumor. In our study, non-V600 mutations were fourfold more likely to metastasize to the abdomen and were less likely to involve the pleura. The mechanism for differential metastatic spread is unclear, but distinct patterns of metastasis have also been reported in other molecular subgroups. For example, rates of brain and pericardial metastases may be higher in *ALK*-positive NSCLC than patients with *EGFR*-mutant and *ROS1*-positive NSCLC [10,11].

This study is inherently limited by its retrospective nature. The sample size was limited by the relative rarity of *BRAF* mutations. As a result, our multivariate model was essentially a comparison between V600-mutant and non-V600-mutant NSCLC. Our study population included patients with both early and advanced stage NSCLC. This may have masked our ability to truly discern differences in primary tumor morphology or sites of metastases that might be more apparent if the analysis were restricted to stage-concordant tumors. We believe that a larger multi-institutional study might overcome these limitations and allow for confirmation of our findings.

In conclusion, this is the largest study to investigate the imaging features of *BRAF*-mutant NSCLC and the first to investigate potential differences in imaging features among the three BRAF functional classes. Our findings suggest that class I (V600) mutated NSCLC may be more likely to have intrathoracic metastases at the time of presentation, while non-V600 (classes II and III) may be more likely to have intra-abdominal metastases.

## Disclosures

**D. Mendoza, T. Chen, A. Padole and S. Rao Digumarthy:** None.
**I. Dagogo-Jack:** Consulting: Boehringer Ingelheim, Honoraria: Foundation Medicine

**A.T. Shaw:** Consultant or received honoraria from: Pfizer, Novartis, Chugai, Genentech/Roche, Ariad/Takeda, Ignyta, LOXO, Blueprint Medicines, KSQ Therapeutics, Daiichi Sankyo, EMD Serono, Taiho Pharmaceutical, TP Therapeutics, Foundation Medicine, Guardant, and Natera. Institutional research funding from: Pfizer, Novartis, Roche/Genentech, Ariad, Ignyta, and TP Therapeutics.

## Conflict of interest

None.

## Appendix A. Supplementary data

Supplementary material related to this article can be found, in the online version, at doi:https://doi.org/10.1016/j.lungcan.2019.01.007.

## References

[1] C.S. Baik, N.J. Myall, H.A. Wakelee, Targeting BRAF-Mutant non-small cell lung Cancer: from molecular profiling to rationally designed therapy, Oncologist 22 (2017) 786–796, https://doi.org/10.1634/theoncologist.2016-0458.
[2] P.K. Paik, M.E. Arcila, M. Fara, C.S. Sima, V.A. Miller, M.G. Kris, M. Ladanyi, G.J. Riely, Clinical characteristics of patients with lung adenocarcinomas harboring

BRAF mutations, J. Clin. Oncol. 29 (2011) 2046–2051, https://doi.org/10.1200/JCO.2010.33.1280.

[3] Z. Yao, R. Yaeger, V.S. Rodrik-Outmezguine, A. Tao, N.M. Torres, M.T. Chang, M. Drosten, H. Zhao, F. Cecchi, T. Hembrough, J. Michels, H. Baumert, L. Miles, N.M. Campbell, E. de Stanchina, D.B. Solit, M. Barbacid, B.S. Taylor, N. Rosen, Tumours with class 3 BRAF mutants are sensitive to the inhibition of activated RAS, Nature 548 (2017) 234–238, https://doi.org/10.1038/nature23291.

[4] A. Noeparast, E. Teugels, P. Giron, G. Verschelden, S. De Brakeleer, L. Decoster, J. De Grève, Non-V600 BRAF mutations recurrently found in lung cancer predict sensitivity to the combination of Trametinib and Dabrafenib, Oncotarget 8 (2016) 60094–60108, https://doi.org/10.18632/oncotarget.11635.

[5] Z. Yao, M. Torres, A. Tao, Y. Gao, L. Luo, Q. Li, E. de Stanchina, O. Abdel-Wahab, D.B. Solit, P. Poulikakos, N. Rosen, BRAF mutants evade ERK-Dependent feedback by different mechanisms that determine their sensitivity to pharmacologic inhibition, Cancer Cell 28 (2015), https://doi.org/10.1016/j.ccell.2015.08.001.

[6] I. Dagogo-Jack, P. Martinez, B.Y. Yeap, C. Ambrogio, L.A. Ferris, C. Lydon, T. Nguyen, N.A. Jessop, A.J. Iafrate, B.E. Johnson, J.K. Lennerz, A.T. Shaw, M.M. Awad, Impact of BRAF mutation class on disease characteristics and clinical outcomes in BRAF-Mutant lung Cancer, Clin. Cancer Res. 2018 (2018), https://doi.org/10.1158/1078-0432.CCR-18-2062 clincanres.2062.

[7] Z. Zheng, M. Liebers, B. Zhelyazkova, Y. Cao, D. Panditi, K.D. Lynch, J. Chen, H.E. Robinson, H.S. Shim, J. Chmielecki, W. Pao, J.A. Engelman, A.J. Iafrate, L.P. Le, Anchored multiplex PCR for targeted next-generation sequencing, Nat. Med. 20 (2014) 1479–1484, https://doi.org/10.1038/nm.3729.

[8] D.F. Halpenny, A. Plodkowski, G. Riely, J. Zheng, A. Litvak, C. Moscowitz, M.S. Ginsberg, Radiogenomic Evaluation Of Lung Cancer – Are There Imaging Characteristics Associated With Lung Adenocarcinomas Harboring BRAF Mutations? Clin. Imaging 42 (2017) 147–151, https://doi.org/10.1016/j.clinimag.2016.11.015.

[9] Z. Cheng, F. Shan, Y. Yang, Y. Shi, Z. Zhang, CT characteristics of non-small cell lung cancer with epidermal growth factor receptor mutation: a systematic review and meta-analysis, BMC Med. Imaging 17 (2017) 5, https://doi.org/10.1186/s12880-016-0175-3.

[10] R.C. Doebele, X. Lu, C. Sumey, D.A. Maxson, A.J. Weickhardt, A.B. Oton, P.A. Bunn, A.E. Barón, W.A. Franklin, D.L. Aisner, M. Varella-Garcia, D.R. Camidge, Oncogene status predicts patterns of metastatic spread in treatment-naive nonsmall cell lung cancer, Cancer 118 (2012) 4502–4511, https://doi.org/10.1002/cncr.27409.

[11] J.F. Gainor, D. Tseng, S. Yoda, I. Dagogo-Jack, L. Friboulet, J.J. Lin, H.G. Hubbeling, L. Dardaei, A.F. Farago, K.R. Schultz, L.A. Ferris, Z. Piotrowska, J. Hardwick, D. Huang, M. Mino-Kenudson, A.J. Iafrate, A.N. Hata, B.Y. Yeap, A.T. Shaw, Patterns of metastatic spread and mechanisms of resistance to crizotinib in ROS1-Positive non–Small-Cell lung Cancer, JCO Precis. Oncol. (2017) 1–13, https://doi.org/10.1200/PO.17.00063.